Journal of the Mechanics and Physics of Solids 107 (2017) 96–114

Contents lists available at ScienceDirect

Journal of the Mechanics and Physics of Solids

journal homepage: www.elsevier.com/locate/jmps

The dependence of the Taylor–Quinney coefficient on the dynamic loading mode

D. Rittel*, L.H. Zhang, S. Osovski

Faculty of Mechanical Engineering, Technion, 32000 Haifa, Israel

ARTICLE INFO

Article history:
Received 2 March 2017
Revised 27 June 2017
Accepted 30 June 2017
Available online 6 July 2017

Keywords:
Taylor–Quinney coefficient
Infrared
Loading mode
Thermomechanical coupling
Kolsky bar

ABSTRACT

The efficiency of the thermomechanical conversion, expressed as the Taylor–Quinney coefficient (TQC) is seldom reported in the literature and generally assumed to be equal to 0.9. Moreover, an eventual dependence of this coefficient on the dynamic loading mode has not been investigated so far.

This work presents a systematic characterization of the TQC for seven different metals and alloys loaded in dynamic tension, compression and dominant shear. The results show that the TQC varies greatly with the investigated material, instead of its assumed constant value of 0.9. Likewise, until final collapse of the specimen, the overall temperature rise remains quite modest.

Moreover, we clearly observe that for commercially pure Titanium, which exhibits an asymmetric mechanical response in tension and compression, the measured TQC values are mode dependent too. Microstructural characterization reveals profuse twinning in compression and shear, as opposed to tension. Twinning is related to heat generation in accord with previous studies.

In addition to reporting a wide database of TQC values, this study reveals a new correlation between the thermomechanical characteristics of a material and its deformation micromechanisms, that should find its way into constitutive models.

1. Introduction

High strain-rate deformation of metallic materials involves a significant release of heat to the surroundings, as a result of the so-called thermomechanical coupling effect by which part of the mechanical work involved in the deformation process is evacuated from the solid as heat. At short time and spatial scales, the process can be considered as adiabatic (Boley and Weiner, 1960), so that the temperature of the solid increases noticeably. While the evolution of heat can occur homogeneously throughout the solid, specific cases of intense strain localization, as in the case of adiabatic shear bands (Dodd and Bai, 2012) can result in spectacular local temperature rise (Duffy and Chi, 1992; Hartley et al., 1987; Marchand and Duffy, 1988).

Starting with the early report of the manifestation of thermomechanical coupling effects in forging (Tresca, 1879), Taylor and co-workers (Farren and Taylor, 1925; Taylor and Quinney, 1934) laid out the foundations of modern thermomechanics by assessing the fraction of mechanical energy that evolves or gets stored in a rapidly deformed solid, universally known as the Taylor–Quinney coefficient. Later works by Dillon (1963) added to the body of knowledge on the subject, and the

* Corresponding author.
E-mail address: merittel@technion.ac.il (D. Rittel).

http://dx.doi.org/10.1016/j.jmps.2017.06.016
0022-5096/

Table 1
Summary of previous measurements of Taylor–Quinney coefficient of metals. Distinction is made between the integral and differential expressions.

Material	Condition	Test	Strain rate /s	β	References
1018 steel	Unspecified	Compression	3000	$>0.80(\beta_{int})$	(Kapoor and Nemat-Nasser, 1998)
4340 steel	Unspecified	Compression	3000	$0.4–0.9(\beta_{diff})$	(Mason et al., 1994)
Ti6Al4V	Unspecified	Torsion	460	$0.2–0.7(\beta_{diff})$	(Macdougall and Harding, 1998)
Ti6Al4V	Unspecified	Compression	3000	$0.5–1.0(\beta_{diff})$	(Mason et al., 1994)
Ti6Al4V	Annealed	Shear	3000	$0.4(\beta_{int})$	(Rittel and Wang, 2008)
CP Ti	Unspecified	Compression	3000	$>0.60(\beta_{int})$	(Kapoor and Nemat-Nasser, 1998)
CP Ti	Unspecified	Compression	3000	$0.75–1.0(\beta_{diff})$	(Hodowany et al., 2000)
Al 2024	Unspecified	Compression	3000	$0.3–1.0(\beta_{diff})$	(Hodowany et al., 2000)
Al 2024	Unspecified	Tension	400	$0.25–0.55(\beta_{diff})$	(Xia and Yao, 1990)
Ta-2.5%W	Unspecified	Compression	3000	$0.4–0.8(\beta_{int})$	(Kapoor and Nemat-Nasser, 1998)
Ta	As-received	Shear	4200	$1.0(\beta_{int})$	(Rittel et al., 2007)
Mg-ED/LD	ECAE	Shear	1800–6000	$0.1–0.3(\beta_{int})$	(Ghosh et al., 2016)
AZ31B-ED	ECAE	Shear	1800–4000	$0.6–0.8(\beta_{int})$	
AZ31B-LD	ECAE	Shear	2600–4000	$0.2–0.6(\beta_{int})$	
AZ31B-TD	ECAE	Shear	2700–3700	$0.5–0.7(\beta_{int})$	

interested reader can find a wealth of references in the seminal review of Bever et al. (1973) on the extent and nature of strain energy storage in metals, also referred to as stored energy of cold work.

While most of the research concentrated on metallic materials, examples of transient thermomechanical measurements on polymers can be found, e.g. in Rittel (1999) and Trojanowski et al. (1997), but such reports are still scarce.

At this stage, it is important to pay attention to the definition of the Taylor–Quinney factor, which expresses the efficiency of the thermomechanical conversion, defined by those authors as the ratio of the thermal *dissipation* to mechanical *work* involved in the deformation process. In the sequel, we will assume adiabatic conditions and neglect thermoelastic couplings. Denoting this factor by β_{int} (integral (Rittel, 1999)) one obtains:

$$\beta_{int} \int^d W_p = \rho c_p \Delta T \tag{1}$$

where $\int dW_p$ is plastic work, ρ is the material density, c_p is the specific heat capacity at constant pressure and ΔT is the temperature rise. β_{int} expresses the fraction of the plastic strain energy density converted into heat. The complementary term, 1- β_{int}, which relates to the stored energy, is directly related to microstructural evolutions through dislocations and twins (Bever et al., 1973).

By contrast, the differential coupled heat equation, as found in Boley and Weiner (1960), involves a ratio of the thermal *rate of dissipation* to mechanical p*ower*, denoted β_{diff} (differential, (Rittel, 1999)), as follows:

$$\beta_{diff} d\dot{W}_p = \rho c_p \dot{T} \tag{2}$$

This ratio is quite different from the integral factor, as it relates to mechanical and thermal powers instead of energies (Rittel, 1999). At this stage, it is important to note that $\beta_{int} \leq 1$, except for the involvement of sources other than plastic dissipation such as latent heat release associated with phase transformations (Rittel et al., 2006a; Zaera et al., 2013). This restriction on β_{int}does not apply to β_{diff}. The sequel of this work will concentrate on the *integral* Taylor–Quinney factor, as an engineering measure of the thermomechanical conversion efficiency.

The determination of β_{int} necessitates the *simultaneous* recording of the stress-strain-temperature of the impacted material. While the determination of the dynamic (compression) characteristics of a material are almost a routine task nowadays, based on the Kolsky (1949) (Split Hopkinson) bar, the transient, non-invasive, measurement of the specimen's temperature is not routinely carried out. For that purpose, infrared detectors have been used with great success, from the early experiments of Hartley et al. (1987), and that technique is the most adequate to-date for transient temperature measurements of the kind discussed here.

As of today, one can only find a few reports of Taylor–Quinney coefficients in the literature, where the values reported by some authors do not always correspond with those reported by other authors on the one hand, or where some confusion as to the integral vs. differential factors persists, under the general denomination of "Taylor–Quinney factor". Table 1 summarizes most of the available references for those factors.

A first observation is that β_{int} is far from being universally equal to 0.9, as commonly assumed for all metallic materials, not to mention a strain and/or strain-rate dependence (Mason et al., 1994; Rittel et al., 2006a), noting that the issue of loading mode was not considered so far. Moreover, from Table 1, it appears that the set of available β_{int} values is quite limited.

Macdougall and Harding (1998) used radiometric techniques and a Cordin 377 high-speed camera to measure the specimen surface temperature and monitor the evolving specimen's cross section of Ti6Al4V alloy specimens in high rate tension and torsion tests. Xia and Rao (1990) designed and manufactured infrared transient temperature-measuring device and investigated the thermomechanically coupled fracture behavior at high rate tension deformation of LY12 Aluminum (equivalent to Al alloy 2024). However, except for these two above-mentioned works, systematic assessments of thermo-

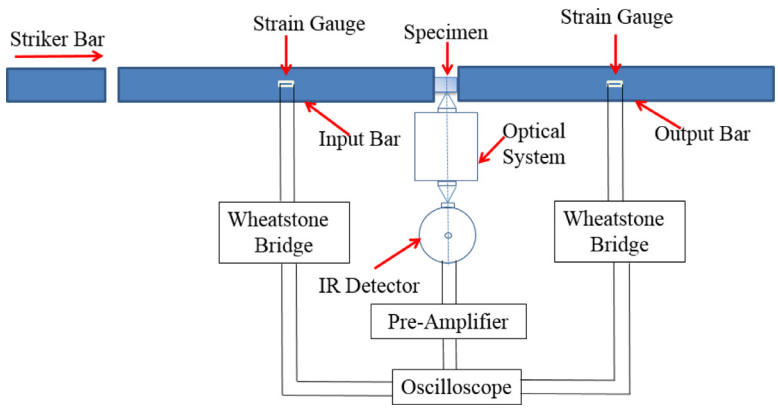

Fig. 1. Schematic representations of the thermomechanical measurement device for a compression experiment.

mechanical aspects in various alloys during high rate tensile deformation are rather scarce, and β_{int}values in dynamic tension are almost non-existent. Moreover, one can note from Table 1 that the vast majority of the experiments carried out so far concern dynamic compression tests, so that the same author(s) did not perform any systematic comparison between tension, compression and shear experiments. A noticeable exception is the recent work of Ghosh et al. (2016), who performed dynamic shear experiments on Magnesium and AZ31B alloy with emphasis on the relationship between the Taylor–Quinney coefficient and microstructural anisotropy.

A related subject is that of adiabatic shear failure, a well-known dynamic failure mechanism, in which failure proceeds by intense shear strain localization in a narrow plane (see e.g. Dodd and Bai, 2012). The classical explanation for the onset of ASB formation, due to Zener and Hollomon (1944), is based on the competition between strain hardening and thermal softening. By contrast, Rittel et al. (2006b) suggested that a critical amount of dynamically stored energy of cold work (SECW) could be viewed as a criterion for the onset of shear localization. This suggestion was based on the observation that the homogenous temperature rise up to the loss of stability was not significant enough to induce a noticeable strain-softening (Rittel and Wang, 2008). Consequently, the determination of the Taylor–Quinney factor, and the corresponding fraction of stored energy of cold work, is of prime importance for the characterization of adiabatic shear band formation from the perspective of the stored energy of cold work this time.

To summarize this brief literature survey, it can be observed that very few results are reported for dynamic tension or shear experiments, and a *systematic comparative study involving dynamic tension, compression and shear of a given material is still missing*. Therefore, the goal of this paper is to report our comparative study for this factor, with all measurements carried out in the same laboratory, using the exact same experimental setup, equipment, specimen geometry and data reduction procedures. While this does not warrant an error-free measurement, the idea is to reduce the scatter in reported values due to measurements usually being carried out in different environments.

In other words, the main goal of this paper is to elucidate whether the Taylor–Quinney coefficient is “universally” independent of the loading mode, and if not, what are the underlying physics.

The paper is therefore organized as follows. We first describe briefly the experimental setup and procedures used to measure the transient temperature evolution of the impacted specimens, including the calibration and data reduction procedures. Next, the materials characterized in this study and the specimens are described, followed by a discussion of the results and concluding remarks.

2. Experimental

2.1. Experimental setup

Fig. 1 is a schematic illustration of the infrared sensing system used in this study for compression experiments. The experimental setup includes two parts: the standard Kolsky compression (and tension) apparatus and the high-speed temperature recording system. The high-speed temperature recording system includes a 1:1 magnification optical system, a high-speed infrared (IR) radiation detector, a signal pre-amplifier and a digital signal acquisition system. Infrared signals are measured using a standard InSb/HgCdTe (MCT) 2-color infrared detector (Infrared Associates Inc.). The MCT photodiode provides optimal responsivity for wavelengths in the range of 5.5–12.5 μm, while the InSb photodiode provides optimal responsivity in the 1–5.5 μm near-infrared region. The active detector’s size is 0.25 mm * 0.25 mm. The experimental setup allows for simultaneous characterization of the thermal and the mechanical processes associated with dynamic deformation. The output signal generated by the strain gauge on the incident bar is used to trigger the digital oscilloscope that records the signals from the high-speed IR detectors. The IR detector is held stationary in front of the specimen and is focused onto the specimen surface. The specimen, optical system and detectors, are all aligned so that a well-defined region on the specimen surface is monitored.

Table 2
Different groups of materials characterized in the present study.

Material	Condition
Commercial Ti6Al4V (Grade 5)	Annealed
Commercial Pure Ti (Grade 2)	Annealed
Al 2024	As-received
Al 5086	As-received
1020 steel	Cold drawn
AISI 304L stainless steel	Cold drawn polished
C300 Maraging steel	Fully hardened

2.2. Thermal data reduction

The technique used to reduce the signal issued from the detector into the specimen's surface temperature has been repeatedly used in Hodowany et al. (2000), Kapoor and Nemat-Nasser (1998), Macdougall and Harding (1998) and will only be briefly outlined here.

A specimen (generally cylindrical) is machined of the material to be tested and instrumented at mid-thickness with a small thermocouple. The calibration procedure consists of heating the instrumented specimen, and then recording simultaneously the IR and thermocouple signals while the specimen is allowed to cool down to room temperature. The sample is placed between the incident and the transmitted bars, and heated using a soldering iron. The procedure is carried out a number of times (typically 5 or more) to ensure repeatability of the calibration curve, as discussed in Rittel et al. (2007). Likewise, additional calibrations are routinely carried out before and after each new test to check again the calibration curve.

The emissivity of the specimen is known to be affected by deformation-induced roughness during dynamic deformation, a point that was not systematically considered here, noting that for strain levels of 0.2 in aluminum (Hodowany et al., 2000), the roughness effect was not found to be significant. Likewise, the variation of the specimen's lateral dimensions (in tension and compression) which might be suspected to influence the focus (and depth of field) of the IR system, was found to be irrelevant for such measurements, as discussed in Regev and Rittel (2008) . Finally, note that the InSb detector, which is especially suitable for higher temperature measurements, was of a lesser usefulness as compared to the MCT detector, but both were used and reported quite comparable temperature changes during impact.

2.3. Materials

Different alloys were characterized in this study, as shown in Table 2.

2.4. Specimens

2.4.1. Compression

Compression specimens were machined into 6 mm diameter and 5 mm length cylinders.

2.4.2. Tension

The tensile specimens' dimensions are shown in Fig. 2.

2.4.3. Dominant shear

The modified SCS specimen (Dorogoy et al., 2015) consists of a cylinder having an inclined gage section created by two semi-circular slots which are machined at 45° with respect to the longitudinal axis. The dimensions of the specimen are shown in Fig. 3. Data reduction for the SCS specimens is carried out as detailed in Dorogoy and Rittel (2005a, b). This includes a preliminary numerical simulation of the specimen to reduce the measured loads and displacements into equivalent stresses and strains in the gauge section.

The total number of tested specimens per loading mode is listed in in Appendix A–C along with the applied strain rate.

3. Results

3.1. Typical experimental results

Typical compression results are introduced here firstly, by taking Ti6Al4V as an example. Fig. 4 shows representative calibration curves for the InSb and MCT channels of the IR detector. The smoothed average line of MCT is used to process the thermal data. Fig. 5 shows the raw data of incident, reflected and transmitted pulses and two signals from detectors during the compression test of Ti6Al4V sample C7 at a room temperature 21.1 °C, and strain rate of 2000/s. The dynamic load equilibrium of the compression specimen is illustrated in Fig. 6, where F-in and F-out stand for incident and transmitted force, respectively. Fig. 7 presents typical plots of the true stress and evolving temperature as a function of the plastic strain

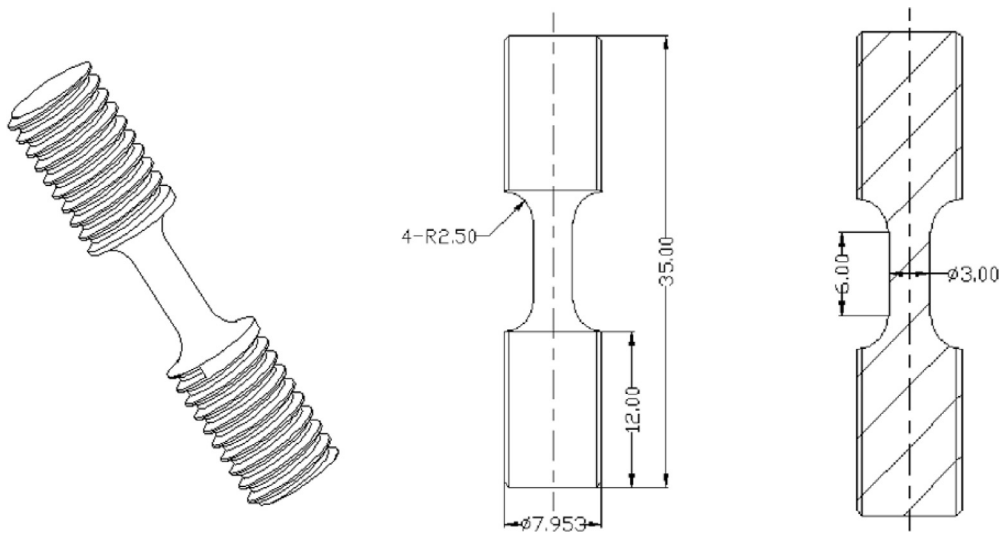

Fig. 2. Geometry of the tensile specimen (all dimension in mm).

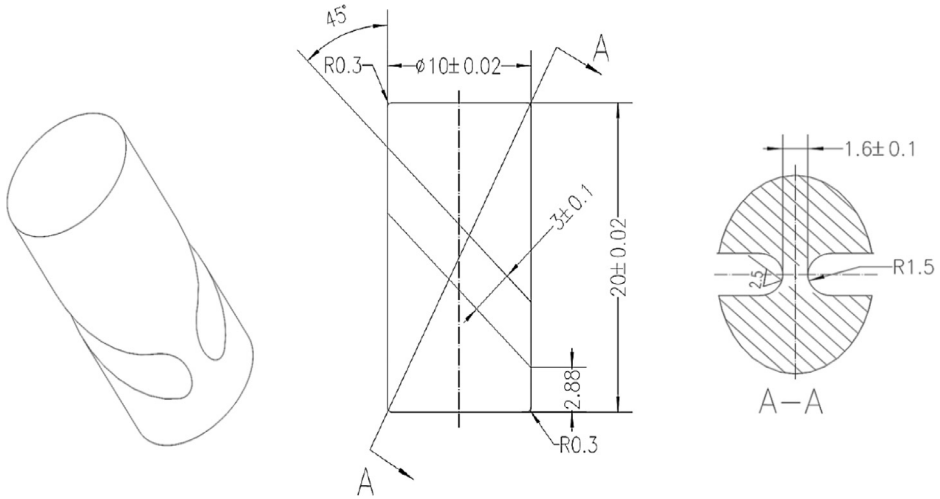

Fig. 3. Shear Compression Specimen (SCS).

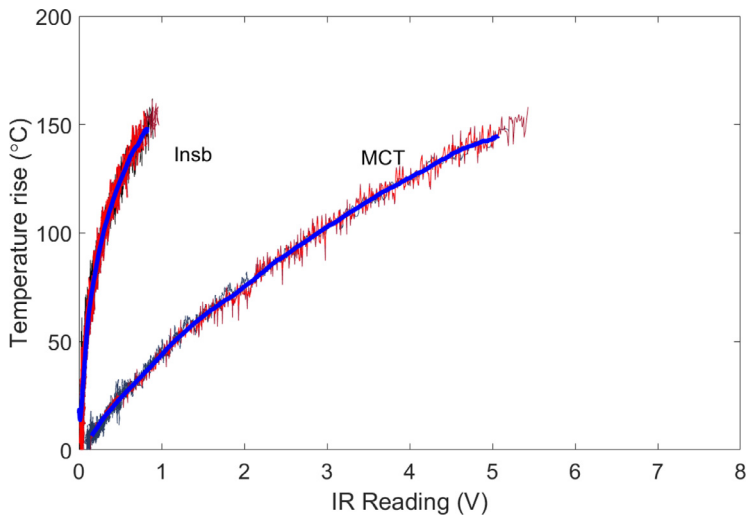

Fig. 4. Typical calibration curves of Ti6Al4V.

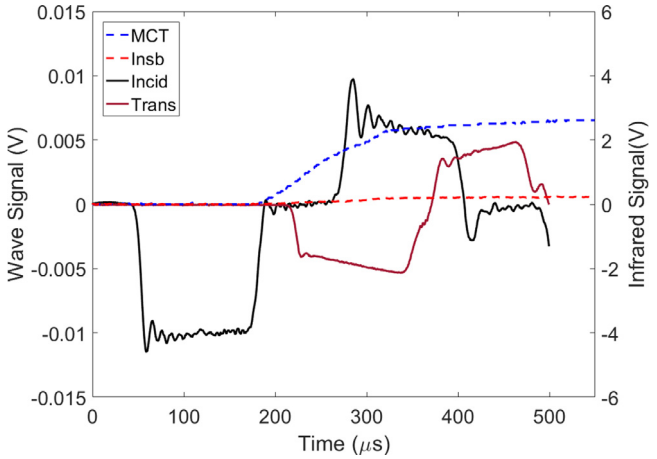

Fig. 5. Raw signals in compression experiment.

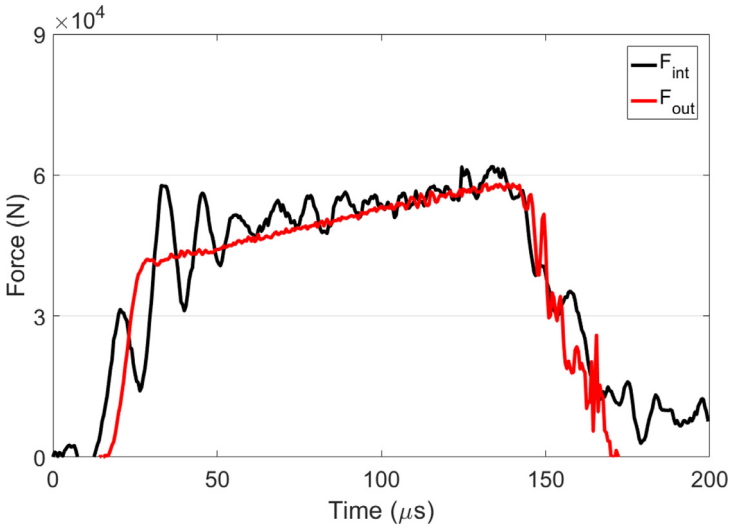

Fig. 6. Force equilibrium in dynamic tension.

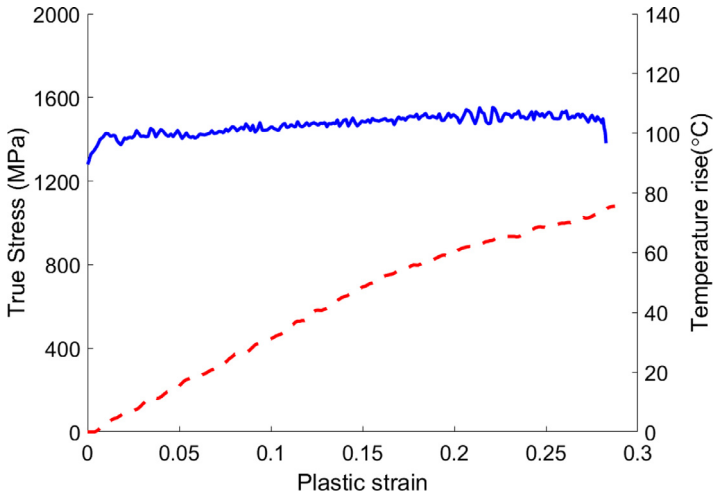

Fig. 7. Typical true stress and temperature rise vs. plastic strain.

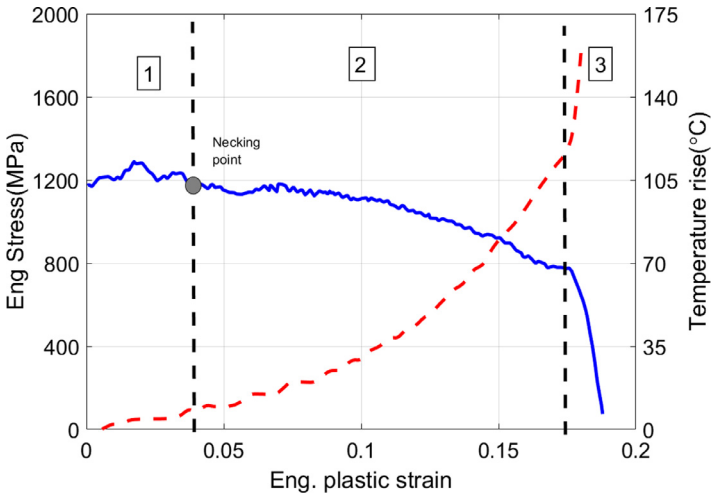

Fig. 8. Typical engineering stress and temperature vs. engineering strain of Ti6Al4V in tension.

for the studied material. The onset of plastic deformation was determined visually as the end of the linear stress-strain domain. The data shown in Fig. 7 is later processed into the Taylor–Quinney coefficient of the experiment.

Next, typical tensile data are shown in Fig. 8.

Fig. 8 shows typical plot of the engineering stress and temperature as a function of the engineering plastic strain for Ti6Al4V at a room temperature 23°C, and strain rate of 1500/s. The choice of engineering measures is motivated by the need to pinpoint the onset of necking in the specimen, which marks a departure from homogeneous plastic deformation. The subsequently reported Taylor–Quinney tensile coefficients concern the homogeneous deformation phase, excluding necking and beyond. Note that prior to the onset of necking, the measured temperature rise remains modest, not exceeding 9 °C, as the overall strain to necking is usually small. Since the temperature measurements reported by Macdougall and Harding (1998) were obtained after fracture of tensile specimens, it is impossible to distinguish between the temperature rise due to uniform plastic deformation, necking localization and the fracturing process, as opposed to the current work. The evolution of the gage temperature in present work is found to comprise three basic stages, in agreement with Xia and Rao (1990) simultaneous observations of mechanical data and gauge deformation patterns. Firstly, prior to necking point, plastic deformation is homogeneous, and the measured stress–strain curve represents the uniform stress status of the deforming gauge section. The temperature increases quite modestly with strain. The second region spans from necking point up to the fracture point, as the macroscopic stress decreases, and the temperature increases noticeably, reaching ~121 °C. Thirdly, roughly at the fracture point, the temperature rise starts to soar up. In addition to the data reported here for Ti6Al4V, these three stages were observed in all dynamic tensile mechanical and thermal response, from the relatively soft Al 2024 to the fully hardened C300 Maraging steel. For the sake of brevity, detailed results for each material are not shown here.

Let us consider shear experiments now. Fig. 9 presents typical plots of the true stress and temperature as a function of the plastic strain at room temperature 25.5 °C and strain rate of 7000/s. Here we mainly consider the temperature rise measured by the MCT detector in the “homogeneous” deformation phase prior to macroscopic onset of localization, indicated by a load drop. The evolution of the gage temperature is found to be in agreement with Rittel and Wang (2008) simultaneous observations of mechanical data and gauge deformation patterns. The temperature increases modestly with the increasing strain prior to macroscopic onset of shear localization. The measured temperature rise at the load drop is ~85 °C corresponding to a homologous temperature of 0.20. In the macroscopic localization phase, the macroscopic stress is decreasing, and the measured temperature grows rapidly and finally soars up to hundred degrees.

3.2. Taylor–Quinney coefficients

The following Figs. 10–17 summarize the integral Taylor–Quinney coefficient β_{int} for each of the investigated materials tested in tension, compression and dominant shear at comparable, although not always identical, strain rates. The results are expressed as average value bounded by the standard error, defined as the standard deviation divided by the square root of the sample size.

Table 3 summarizes the measured coefficients for each loading mode.

Table 3 and Fig. 17 clearly show that, whereas most investigated materials exhibit rather similar β_{int}, CP-Ti is characterized by a marked sensitivity to the loading mode, with high compression and shear values of the Taylor–Quinney factor, as opposed to tension.

To elucidate the underlying reasons for this discrepancy, CP-Ti specimens, which were subjected to the three different loading modes considered here, were subjected to microstructural characterisation (Fig. 18). The specimens were polished

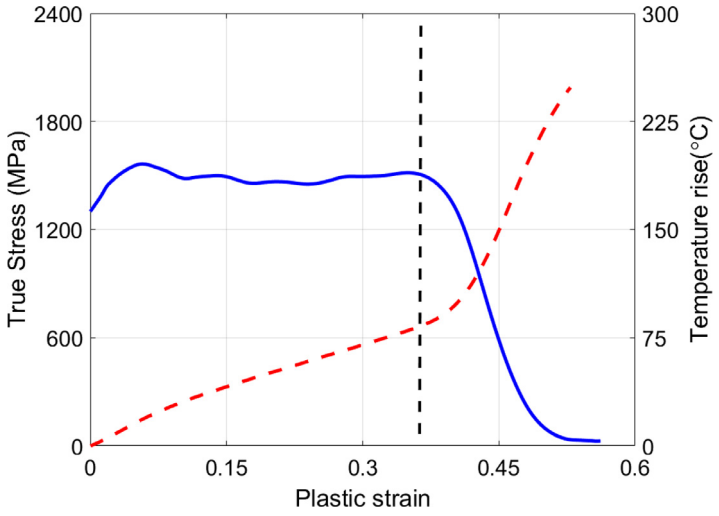

Fig. 9. Typical equivalent stress and tempeature vs. plastic strain for Ti6Al4V in shear.

Table 3
Comparison of average β_{int} (Min-Max of solid line in Fig. 12–18) for three loading modes for each material.

Material	$\boldsymbol{\beta_{int}}$	Compression	Tension	Shear	
Ti6Al4V	Strain rate	2000/s	1500–3400/s	2800/s	5000–7000/s
	β_{int}	0.4–0.5	0.30–0.40	0.4–0.5	0.36–0.45
CP Ti	Strain rate	2000–3000/s	600–900/s, 2000–2500/s	3300/s,3500/s,5000/s	
	β_{int}	0.71–0.96	0.44–0.65	0.79–0.84	
Al 5086	Strain rate	2200–2500/s	2000–3000/s	5000/s	
	β_{int}	0.20–0.40	0.20–0.37	0.18–0.39	
Al2024	Strain rate	2500–3000/s	1250–1600/s	5000/s	
	β_{int}	0.20–0.25	0.25–0.35	0.22–0.40	
304L	Strain rate	2000–2800/s	1750–2000/s	7000/s	
	β_{int}	0.50–0.70	0.44–0.57	0.40–0.73	
1020 steel	Strain rate	1300–1500/s	1400–2000/s	4000/s–6000/s	
	β_{int}	0.82–0.92	0.80–0.87	0.80–0.92	
C300	Strain rate	1200–1800/s	1000–2500/s	1500–2500/s	
	β_{int}	0.49–0.60	0.38–0.50	0.41–0.53	

using the standard procedures and etched using Kroll's reagent to reveal the deformed microstructures. The three specimens presented in Fig. 18 correspond to a fractured shear specimen with a plastic strain of 0.3, an unfractured compression specimen (1C1) deformed to a plastic strain of 0.25, and the neck region of an unfractured tension specimen (1T7) deformed to an equivalent strain of 0.25. Here, the equivalent strain in the necking region is calculated by carefully measuring the radius of the minimum cross-section.

The initial microstructure of the CP Ti consisting of alpha phase is presented in Fig. 18(A). For the shear specimen, Fig. 18(B), the grains are elongated and profuse twinning is evident, just like for the compression specimen of Fig. 18(C). In both shear and compression configurations, the twins are evenly distributed in the characterized cross-section. By contrast, the tensile specimen of Fig. 18(D) exhibits only very few twins. Although the strain levels of the specimens under the three loading modes are not exactly identical, Fig. 18 undoubtly reveals the dominant presence of twins in the shear and compression specimens, as opposed to the tensile one.

4. Discussion

The current research was primarly driven by the scarcity and dicrepancies of experimental data in the literature, regarding the thermo-mechanical properties of structural alloys and metals subjected to high rate deformation. The result of this knowledge gap is that the majority of theoretical and numerical studies on high rate deformation found in the literature, have resorted to assuming a constant value of the Taylor–Quinney coefficient, regardless of the material in question and its loading path, while disregarding the available experimental data. To elucidate that and explore the potential differences in the Taylor–Quinney coefficient for different materials and loading modes, we have conducted a systematic experimental exploration of this value for 7 different structural alloys, under three loading modes (i.e. compression, tension, and dominant shear).

The first and possibly most important outcome of this effort, is a unified database regarding the thermomechanical heat conversion factor β_{int}. To the best of our knowledge it is the first time a systematic exploration of β_{int} is performed

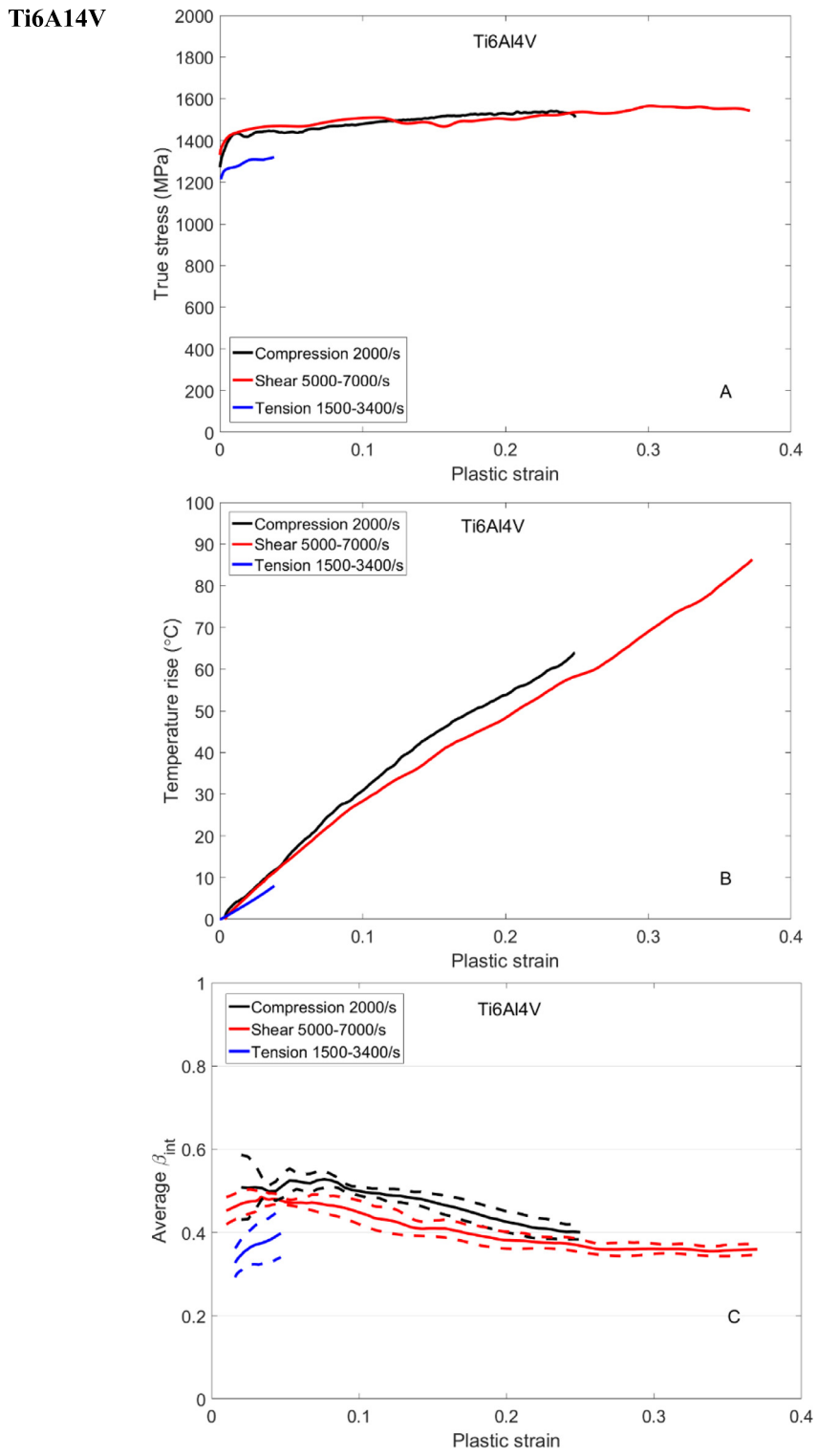

Fig. 10. Average results of Ti6Al4V. (A) Average true stress vs. plastic strain, (B) Average temperature rise vs. plastic strain, (C) Average β_{int} vs. plastic strain. The curves are expressed as average β_{int} (solid) $\pm$ standard error (dashed).

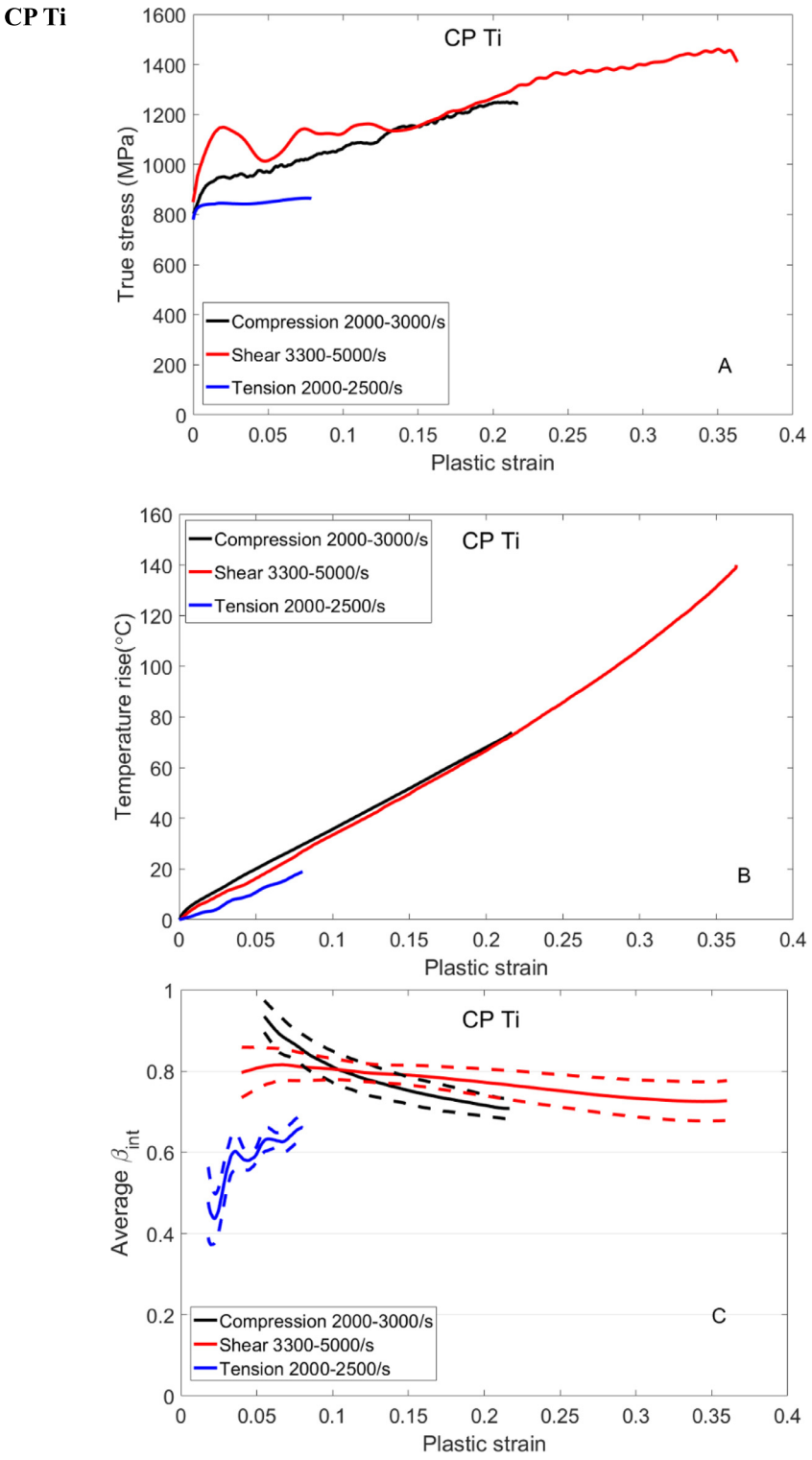

Fig. 11. Average results of CP Ti. (A) Average true stress vs. plastic strain, (B) Average temperature rise vs. plastic strain, (C) Average β_{int} vs. plastic strain. The curves are expressed as average β_{int} (solid) $\pm$ standard error (dashed).

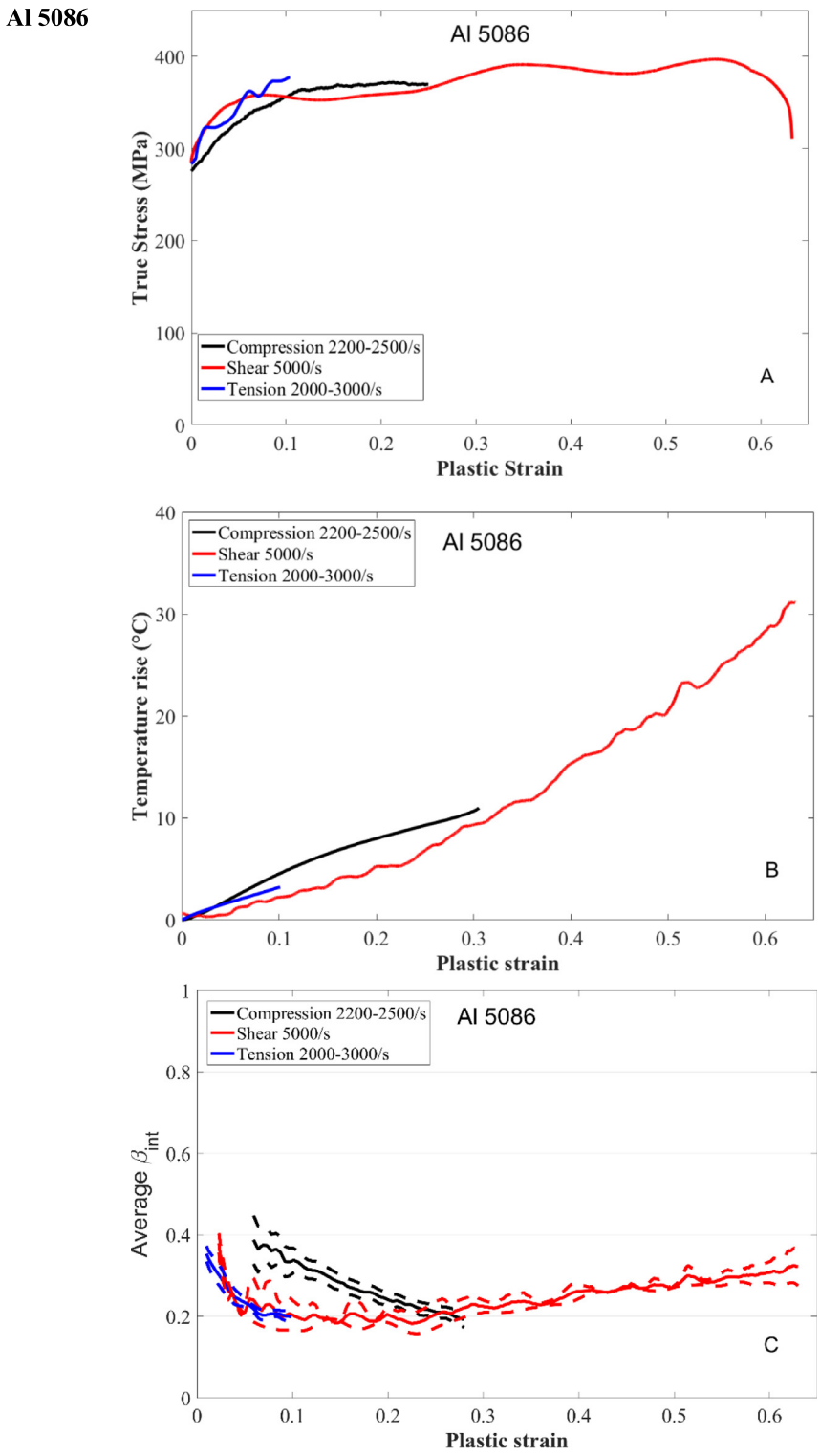

Fig. 12. Average results of Al 5086. (A) Average true stress vs. plastic strain, (B) Average temperature rise vs. plastic strain, (C) Average β_{int} vs. plastic strain. The curves are expressed as average β_{int} (solid) $\pm$ standard error (dashed).

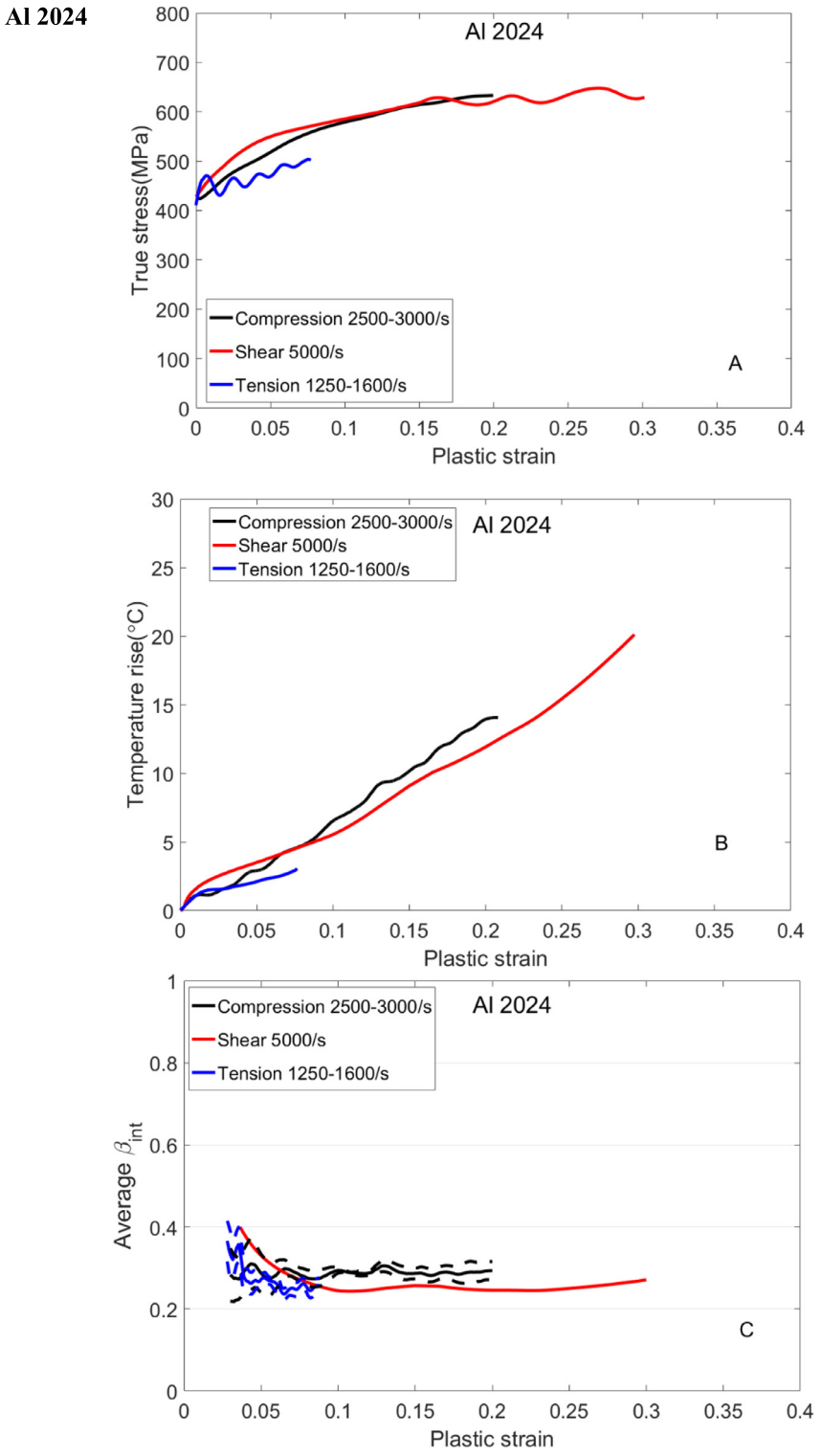

Fig. 13. Average results of Al 2024. (A) Average true stress vs. plastic strain, (B) Average temperature rise vs. plastic strain, (C) Average β_{int} vs. plastic strain. The curves are expressed as average β_{int} (solid) $\pm$ standard error (dashed).

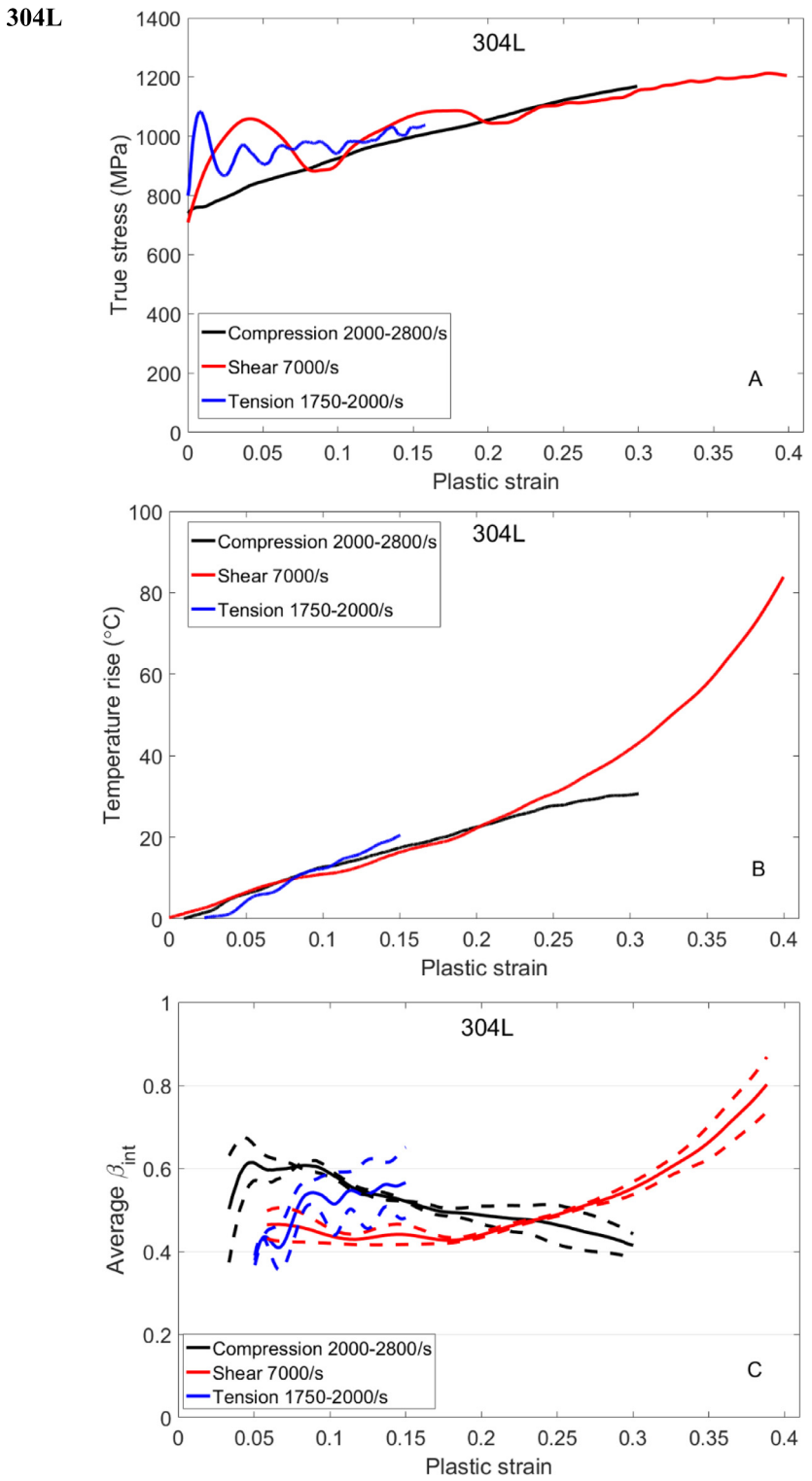

Fig. 14. Average results of 304L. (A) Average true stress vs. plastic strain, (B) Average temperature rise vs. plastic strain, (C) Average β_{int} vs. plastic strain. The curves are expressed as average β_{int} (solid) $\pm$ standard error (dashed).

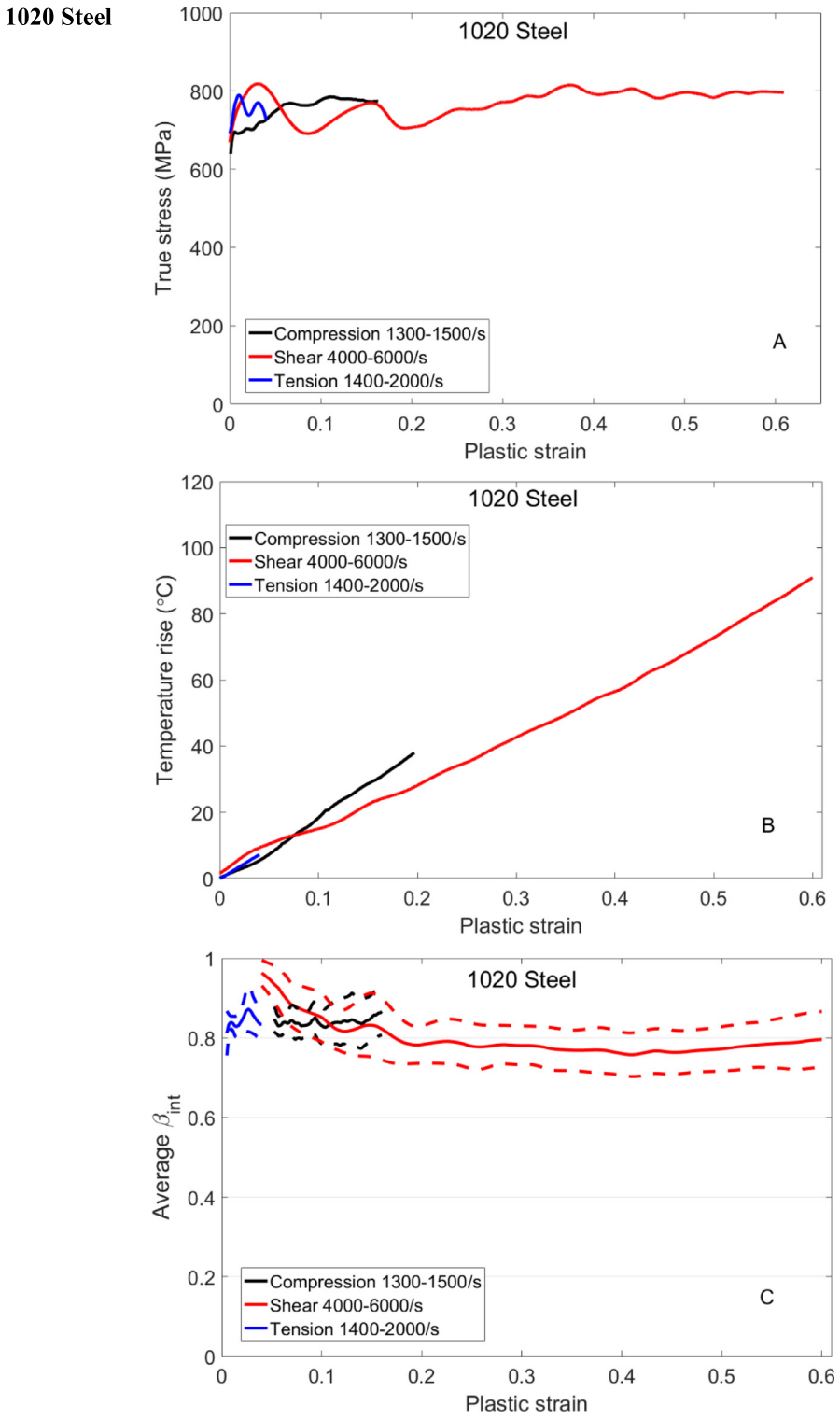

Fig. 15. Average results of 1020 Steel. (A) Average true stress vs. plastic strain, (B) Average temperature rise vs. plastic strain, (C) Average β_{int} vs. plastic strain. The curves are expressed as average β_{int} (solid) $\pm$ standard error (dashed).

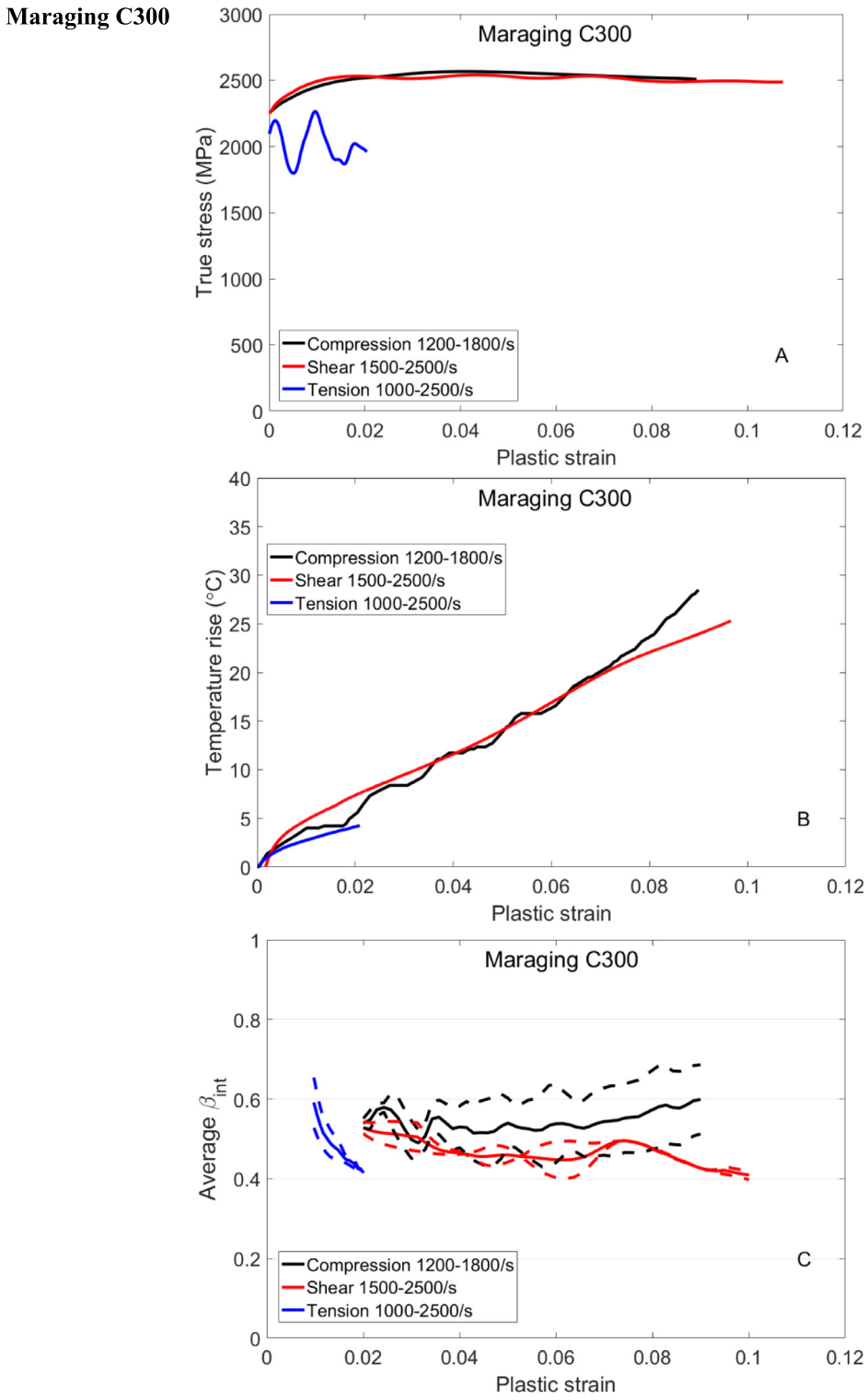

Fig. 16. Average results of Maraging C300 Steel. (A) Average true stress vs. plastic strain, (B) Average temperature rise vs. plastic strain, (C) Average β_{int} vs. plastic strain. The curves are expressed as average β_{int} (solid) $\pm$ standard error (dashed).

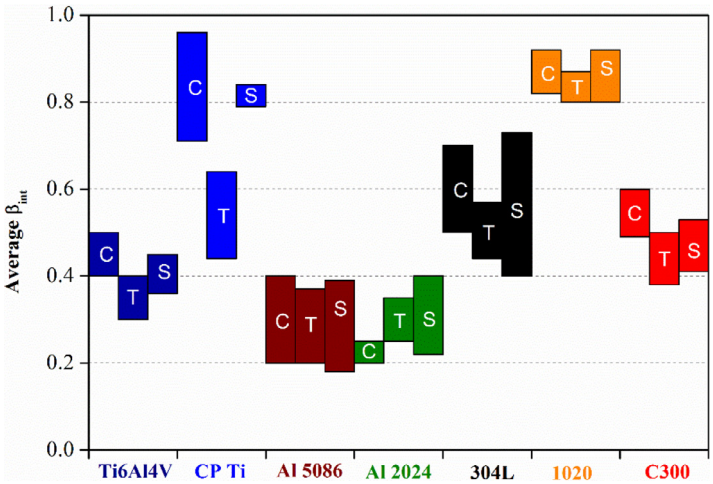

Fig. 17. Plot of average β_{int} for each material to illustrate Table 3 under Compression-Tension-Shear(C-T-S).

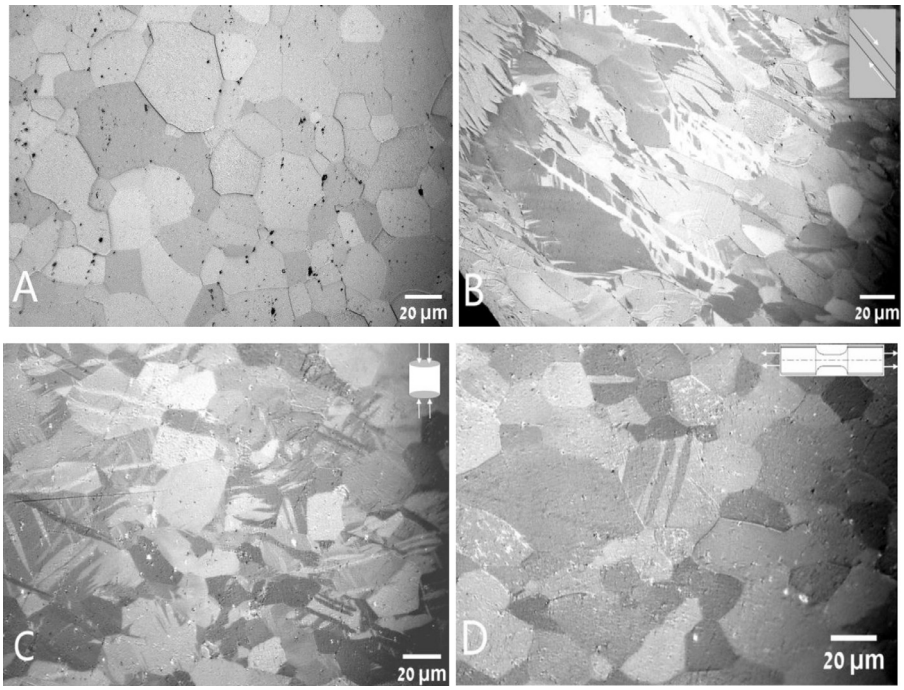

Fig. 18. Microstructures of CP-Ti under three loading modes (Kroll etchant). (A) Initial microstructure, (B) Shear failed specimen 1S3, $\varepsilon_p = 0.37$, (C) Compression deformed specimen 1C1, $\varepsilon_p = 0.25$ (D) Unbroken tension specimen 1T7, $\varepsilon_p = 0.25$.

covering several materials all measured using the same technique and under the same loading conditions. As a result, this database can be used for comparative theoretical and numerical studied regarding the high rate deformation and failure (e.g. through adiabatic shear localization) of the materials at questions.

Next, considering the evolution of β_{int} with imposed strain, it is apparent that while for some materials and loading modes β_{int} remains quite constant (within experimental accuracy), for others, a significant variation can be observed (see for example Fig. 14 where the β_{int} values measured for 304L stainless steel are presented). This topic merits a separate investigation as to the microstructural evolution under different deformation modes and the resulting failure mechanisms and mechanical behavior. It is plausible that, by varying the microstructural constituents of a material and studying the resulting thermomechanical conversion factor with regards to the microstructural evolution, a better paradigm for controlling catastrophic failure events such as adiabatic shear localization could be devised.

Keeping that in mind, let us take more detailed look into the thermomechanical data presented in Fig. 11 for CP-Ti, where the values of the Taylor–Quinney coefficient are presented for compression ($0.7 \leq \beta_{int} \leq 0.9$) dominant shear ($0.72 \leq$

$\beta_{int} \leq 0.81$) and tension ($0.44 \leq \beta_{int} \leq 0.65$). While it is well known that pure Ti displays an asymmetry in its mechanical properties (Revil-Baudard et al., 2015), due to the activation of deformation twins, a direct experimental evidence that the energy storage (or heat dissipation) stemming from the two different mechanisms is significantly different is presented here for the first time. The lower value of β_{int} measured for the tension experiments correlates with the deformed microstructure observed in Fig. 18 where the amount of deformation twins observed in the tensile specimen is significantly less than that in shear and compression. Similar claims were made by Padilla et al. (2007) were it was claimed that the formation of twin boundaries doesn't store any significant level of energy. The experimental evidence for the lack of energy storage capability of deformation twins, presented her, further support the conclusions of Osovski et al. (2013) where this phenomena was assumed and used to explain the late appearance of dynamically recrystallized grains in CP-Ti when compared to Ti6Al4V alloy.

The results presented here suggest that the common approach for studying the process of adiabatic shear banding, in which thermal softening is taken to be the major player, should be reconsidered (at least for some of the materials in question) in light of the measured values of β_{int} which are noticeably smaller than the commonly assumed value of 0.9, while validating at the same time this assumption for other materials (Molinari and Clifton, 1987).

Finally, beyond its relevance to adiabatic shear banding, the stored energy of cold work (SECW) has a definite relevance in a wealth of physical phenomena such as recrystallization, phase changes and residual stresses, as surveyed in Bever et al. (1973). The present study reports both basic data and a simple methodology to determine the SECW, with special care being paid to the deformation micromechanisms and the various loading modes.

5. Conclusions

We have presented here an experimental study as to the thermal response of several structural alloys subjected to dynamic loading. Seven different materials were considered under three distinct deformation modes, thus providing a unified database for those materials. The non-universal value of the Taylor–Quinney coefficient was demonstrated as well as its dependence on strain and loading mode (for some materials). In addition, a direct experimental evidence for the lack of energy storage in twin mediated plasticity was found for CP Ti.

Finally, from a practical design approach, the importance of generating a similar database for a larger group of materials, to be used in computer simulations, and possibly for future directions in materials design against dynamic loading, was demonstrated.

Acknowledgments

The authors thank Mr. Y. Rositzky, Mr. A. Reuben, Mr. Y. Meshali, Dr. A. Dorogoy, Mr. D. Zolotaryov and Mr. Y. Rotbaum for their technical assistance. The support of the Israel Science Foundation (Grant 1034/13) is kindly acknowledged.

Appendix A. Compression

No.	Material	Sample	Length-Diameter (mm)	Strain rate (/s)	Fracture (Y/N)
1	Ti6Al4V	C4	5.01-6.01	2000	N
2		C5	5.02-6.00	2000	N
3		C7	5.02-6.01	2000	N
4		C9	5.02-6.01	1200	N
5	CP Ti	C1	5.00-5.95	2000	N
6		C2	4.96-5.98	2200	N
7		C3	4.96-5.98	1750	N
8		C6	4.97-6.00	3000	N
9	Al 2024	C2	4.99-5.98	2500	N
10		C7	5.02-6.02	2750	N
11		C9	5.47-5.97	3000	N
12		C10	4.99-6.01	3000	N
13	Al 5086	C1	5.97-5.95	2200	N
14		C2	5.99-5.99	2200	N
15		C3	5.97-6.00	2200	N
16		C8	3.98-6.03	2500	N
17	1020 steel	C2	5.04-10.06	1300	N
18		C6	5.00-10.01	1300	N
19		C7	4.95-9.98	1500	N
20		C8	5.06-10.00	1300	N
21		C10	5.01-10.06	1500	N
22	304L	C2	4.00-6.00	2800	N
23		C4	5.00-6.00	2700	N
24		C5	5.01-6.00	2000	N
25	C300	C6	5.01-5.93	1800	Y
26		C7	4.96-5.98	1700	Y
27		C8	5.02-6.01	1500	Y
28		C11	5.02-6.03	1200	Y

Appendix B. Tension

No.	Material	Sample	Length-Diameter (mm)	Strain rate (/s)	Fracture (Y/N)
1	Ti6Al4V	T1	6.25-3.00	3400	Y
2		T2	6.00-3.01	2750	Y
3		T3	6.00-2.97	1500	Y
4		T4	6.20-2.98	2750	Y
5	CP Ti	T1	5.00-3.01	2250	Y
6		T4	5.50-2.98	2500	Y
7		T6	5.15-2.99	2000	Y
8		T7	4.86-2.98	900	N
9		T10	5.00-3.00	600	N
10	Al 2024	T1	6.50-2.98	1250	Y
11		T3	6.65-2.94	1500	Y
12		T4	6.00-2.96	1600	Y
13		T7	6.08-2.98	1400	Y
14	Al 5086	T1	6.20-2.97	2000	Y
15		T2	6.49-2.97	3000	Y
16		T3	6.55-2.95	2000	Y
17		T4	6.61-2.97	2000	Y
18	1020 steel	T1	6.15-3.00	1500	Y
19		T2	6.81-2.98	1400	Y
20		T3	6.10-2.99	1900	Y
21		T4	6.24-2.95	2000	Y
22		T5	6.32-2.99	1600	Y
23	304L	T2	6.53-3.01	1750	N
24		T4	6.42-2.99	2000	N
25		T5	6.73-3.01	2000	N
26	C300	T1	6.57-2.99	1000	Y
27		T4	6.19-2.99	1250	Y
28		T5	6.22-2.99	1000	Y

Appendix C. Dominant shear

No.	Material	Sample	H-D-t-W (mm)	Strain rate (/s)	Fracture (Y/N)
1	Ti6Al4V	S1	19.99-10.02-1.65-3.19	7000	Y
2		S3	20.01-10.00-1.65-3.15	7000	Y
3		S4	19.95-9.99-1.55-3.12	5000	Y
4		S5	19.98-10.00-1.64-3.17	2800	N
5		S7	20.06-10.04-1.46-3.17	7000	Y
6	CP Ti	S3	20.00-10.00-1.54-3.12	4000	Y
7		S4	20.02-10.01-1.55-3.08	3500	Y
8		S7	20.01-9.99-1.50-3.16	4000	Y
9		S8	20.01-10.00-1.53-3.09	3300	Y
10		S10	20.02-10.01-1.60-3.19	5000	Y
11	Al 2024	S3	30.28-16.7-2.70-5.30	5000	Y
12	Al 5086	S8	20.00-10.00-1.39-3.28	5000	N
13		S10	20.00-9.99-1.40-3.05	5000	N
14	304L	S7	19.98-9.99-1.53-3.08	7000	Y
15		S8	20.00-10.00-1.58-3.12	7000	Y
16		S10	19.98-10.00-1.50-3.18	7000	Y
17	1020 steel	S1	19.97-9.98-1.50-3.10	4000/s	N
18		S5	20.02-9.98-1.5-3.00	5500/s	N
19		S10	19.98-9.97-1.45-3.06	6000/s	N
20	C300	S5	19.99-10.00-2.24-3.00	1500/s	Y
21		S6	19.98-10.05-1.84-2.50	2500/s	Y
22		S8	19.98-10.00-1.83-2.55	2000/s	Y
23		S11	19.76-9.96-1.60-2.52	6500/s	Y

References

Bever, M.B., Holt, D.L., Titchener, A.L., 1973. The stored energy of cold work. Prog. Mater. Sci. 17, 5–177.
Boley, B.A., Weiner, J.H., 1960. Theory of Thermal Stress.
Dillon, O.W., 1963. Coupled thermoplasticity. J. Mech. Phys. Solids 11, 21–33.
Dodd, B., Bai, Y., 2012. Adiabatic Shear Localization: Frontiers and Advances. Elsevier, Amsterdam.
Dorogoy, A., Rittel, D., 2005a. Numerical validation of the shear compression specimen. Part 1: quasi-static large strain testing. Exp. Mech. 45, 167–177. doi:10.1177/0014485105052325.
Dorogoy, A., Rittel, D., 2005b. Numerical validation of the shear compression specimen. Part II: dynamic large strain testing. Exp. Mech. 45, 178–185. doi:10.1177/0014485105052324.

Dorogoy, A., Rittel, D., Godinger, A., 2015. Modification of the shear-compression specimen for large strain testing. Exp. Mech. 55, 1627–1639. doi:10.1007/s11340-015-0057-6.
Duffy, J., Chi, Y.C., 1992. On the measurement of local strain and temperature during the formation of adiabatic shear bands. Matls. Sci. Eng. A 157, 195–210.
Farren, W.S., Taylor, G.I., 1925. The heat developed during plastic extension of metals. Proc. R. Soc. A107, 422–451.
Ghosh, D., Kingstedt, O.T., Ravichandran, G., 2016. Plastic work to heat conversion during high-strain rate deformation of Mg and Mg alloy. Metall. Mater. Trans. A 48, 14–19. doi:10.1007/s11661-016-3825-8.
Hartley, K.A., Duffy, J., Hawley, R.H., 1987. Measurement of the temperature profile during shear band formation in steels deforming at high strain rates. J. Mech. Phys. Solids 35, 283–301.
Hodowany, J., Ravichandran, G., Rosakis, A.J., Rosakis, P., 2000. Partition of plastic work into heat and stored energy in metals. Exp. Mech. 40, 113–123.
Kapoor, R., Nemat-Nasser, S., 1998. Determination of temperature rise during high strain rate deformation. Mech. Mater. 27, 1–12.
Kolsky, H., 1949. An investigation of the mechanical properties of materials at very high rates of loading. Proc. Phys. Soc. Sect. B 62, 676.
Macdougall, D.A.S., Harding, J., 1998. The measurement of specimen surface temperature in high-speed tension and torsion tests. Int. J. Impact Eng. 21, 473–488.
Marchand, A., Duffy, J., 1988. An experimental study of the formation process of adiabatic shear bands in a structural steel. J. Mech. Phys. Solids 36, 251–283.
Mason, J.J., Rosakis, A.J., Ravichandran, G., 1994. On the strain and strain rate dependence of the fraction of plastic work converted into heat: an experimental study using high speed infrared detectors and the Kolsky bar. Mech. Mater. 17, 135–145.
Molinari, A., Clifton, R.J., 1987. Analytical characterization of the shear localization in thermoviscoplastic materials. J. Appl. Mech. 54, 806–812.
Osovski, S., Rittel, D., Venkert, A., 2013. The respective influence of microstructural and thermal softening on adiabatic shear localization. Mech. Mater. 56, 11–22. doi:10.1016/j.mechmat.2012.09.008.
Padilla, H.A., Smith, C.D., Lambros, J., Beaudoin, A.J., Robertson, I.M., 2007. Effects of deformation twinning on energy dissipation in high rate deformed zirconium. Metall. Mater. Trans. A 38A, 2916–2927.
Regev, A., Rittel, D., 2008. Simultaneous transient temperature sensing of impacted polymers using infrared detectors and thermocouples. Exp. Mech. 48, 675–682.
Revil-Baudard, B., Cazacu, O., Flater, P., Kleiser, G., 2015. Plastic deformation of high-purity α-titanium: model development and validation using the Taylor cylinder impact test. Mech. Mater. 80, 264–275. doi:10.1016/j.mechmat.2014.03.010.
Rittel, D., 1999. On the conversion of plastic work to heat during high strain rate deformation of glassy polymers. Mech. Mater. 31, 131–139.
Rittel, D., Bhattacharyya, A., Poon, B., Zhao, J., Ravichandran, G., 2007. Thermomechanical characterization of pure polycrystalline tantalum. Matls. Sc. Engng. A A447, 65–70. doi:10.1016/j.msea.2006.10.064.
Rittel, D., Ravichandran, G., Venkert, A., 2006a. The mechanical response of pure iron at high strain rates under dominant shear. Matls. Sc. Engng. A A432, 191–201. doi:10.1016/j.msea.2006.05.154.
Rittel, D., Wang, Z.G., 2008. Thermo-mechanical aspects of adiabatic shear failure of AM50 and Ti6Al4V alloys. Mech. Mater. 40, 629–635. doi:10.1016/j.mechmat.2008.03.002.
Rittel, D., Wang, Z.G., Merzer, M., 2006b. Adiabatic shear failure and dynamic stored energy of cold work. Phys. Rev. Lett. 96, 75502. doi:10.1103/PhysRevLett.96.075502.
Taylor, G.I., Quinney, H., 1934. The latent energy remaining in a metal after cold working. Proc. R. Soc. London 143, 307–326.
Tresca, H., 1879. Sur la fluidité et l'écoulement des corps solides. Ann. du Conserv. des Arts Métiers, p. 4.
Trojanowski, A., Ruiz, C., Harding, J., 1997. Thermomechanical properties of polymers at high rates of strain. J. Phys. Coll. C 3, 447–452.
Xia, Y., Rao, S., 1990. An infrared transient temperature measuring apparatus and its application to the tensile impact testing. Chin. J. Exp. Mech. 5, 170–177.
Zaera, R., Rodríguez-Martínez, J.A., Rittel, D., 2013. On the Taylor–Quinney coefficient in dynamically phase transforming materials. Application to 304 stainless steel. Int. J. Plast. 40, 185–201.
Zener, C., Hollomon, J.H., 1944. Effect of strain rate upon plastic flow of steel. J. Appl. Phys. 15, 22–32.